LANGMUIR Article
Cite This: Langmuir XXXX, XXX, XXX−XXX
pubs.acs.org/Langmuir

Infrared Absorption Spectroscopy of Albumin Binding with Amine-Containing Plasma Polymer Coatings on Nanoporous Diamond Surfaces

Halyna Kozak,*[,†] Anna Artemenko,[†] Egor Ukraintsev,[†] Andrei Choukourov,[‡] Bohuslav Rezek,[†,§] and Alexander Kromka[†]

[†]Institute of Physics, Czech Academy of Sciences, 162 00 Prague 6, Czech Republic
[‡]Faculty of Mathematics and Physics, Charles University, 18000 Prague 8, Czech Republic
[§]Faculty of Electrical Engineering, Czech Technical University, 166 27 Prague 6, Czech Republic

Supporting Information

ABSTRACT: Nanocrystalline diamond (NCD) layers functionalized with amine-containing functional groups have generated considerable interest as biocompatible substrates for attachment of biomolecules and cells with a view to biosensor and tissue engineering applications. Here we prepare nanoporous diamond layers with the surfaces modified by hydrogen plasma, oxygen plasma, and conformal 7 nm amine-containing plasma polymer (PP). Immobilization of bovine serum albumin (BSA) molecules is characterized on such surfaces. Grazing angle reflectance infrared spectroscopy as well as X-ray photoelectron spectroscopy show that concentration of amine-containing bonds after BSA exposure depends on the type of NCD surface modification. AFM measurements reveal that BSA proteins are physisorbed on H- and O-terminated diamond surfaces in different thicknesses and morphology. When the diamond layers are coated with the amine-containing PP, BSA molecules assume similar thickness and morphology, and their adhesion is significantly increased on both types of the diamond surfaces.

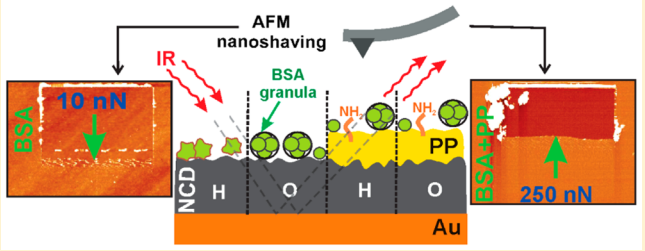

INTRODUCTION

Diverse biomaterials and nanomaterials have become increasingly useful as passive substrates or electrically active platforms for monitoring and modifying biological interactions and biochemical reactions. Diamond due to a unique combination of physical, chemical, mechanical, and optical properties[1,2] is very attractive material for such applications, from biosensors to tissue engineering. It is also known as functional with high durability, physical and chemical inertness, and high compatibility with many specific organic molecules.[3] The surface of diamond can be relatively easily terminated by various functional groups resulting in a change of its wettability and chemical and electrical properties. Depending on the application and the desired physical and chemical properties of the diamond surface, different strategies for covalent diamond functionalization such as hydrogenation, amination, oxidation, fluorination, halogenation, and carboxylation have been proposed.[4] An increasing popular method of changing diamond surface properties is a plasma modification, which provides an economical and effective way to uniformly modify surfaces of various dimensions. Hydrogen and oxygen plasma treatments are two common diamond surface modifications. Hydrogen plasma produces hydrophobic diamond surface with negative electron affinity and surface conductivity of the p-type even without any doping.[5] An oxygen terminated diamond surface, in contrast, remains isolating, is hydrophilic and has a positive electron affinity.[6] This is due to a difference in the dipole moments of C−H and C−O bonds on the diamond surface. This dipole moment can play a crucial role in a selective attraction of biomolecules and/or increasing their covalent immobilization on the diamond surface. It was demonstrated that the hydrogen and oxygen plasma treatments change the wettability of the diamond surface and influence osteoblast cell (SAOS-2) arrangement and growth on the diamond micropatterns.[7]

In particular, the functionalization with amine-containing functional groups, primary amines for example, is another important termination of the diamond surfaces enabling preparation of the chemically reactive platforms for covalent immobilization of biomolecules.[8,9] In the literature, two main approaches for the functionalization of the diamond surface with amino functional groups can be found. The first one is based on a direct radio frequency (RF) plasma treatment in pure ammonia (NH_3) or NH_3/N_2 working gas mixtures.[8,10] A second possibility is a coating of the diamond surface by a thin amine-containing polymer film that provides a homogeneous

Received: July 25, 2019
Revised: September 21, 2019
Published: September 24, 2019

Downloaded via NORTHWESTERN UNIV on October 21, 2019 at 22:13:40 (UTC).
See https://pubs.acs.org/sharingguidelines for options on how to legitimately share published articles.

© XXXX American Chemical Society

DOI: 10.1021/acs.langmuir.9b02327
Langmuir XXXX, XXX, XXX−XXX

and chemically stable interface for the attachment of biomolecules.[11,12] Recently, we have shown that the surface of nanocrystalline diamond (NCD) layers can be modified by the deposition of amine-containing plasma polymer.[13] It was shown that the plasma polymer (PP) deposited on the NCD surface contains a five times higher concentration of nitrogen and more than four times higher amount of $-NH_2$ groups (5%) than the NCD treated by the NH_3 plasma (1%). Moreover, the surface conductivity of H-NCD after the deposition of PP was preserved with a value of about 10^{-7} S.[13] According to our previous results this value is high enough for biosensor applications[14,15] However, there is still a lack of information about how the amination of the diamond surface by PP alters the extent of the protein adsorption. Protein adsorption is a key factor for controlling the cell−surface interactions, since the cells are directly interacting with the cell adhesive proteins.[16,17]

Fourier transform infrared (FTIR) spectroscopy is one of the fundamental analytical techniques for a detailed analysis of surface chemistry. It has been widely used to analyze the chemical composition and structure of different nucleic acids, proteins, living cells, and other biomolecules.[18,19] The most commonly used FTIR reflection techniques are attenuated total reflectance (ATR) and grazing angle reflectance (GAR) spectroscopy. ATR-FTIR is based on a measuring the optical absorption of the evanescent wave which occurs in a totally internally reflected infrared beam when the sample is attached to the prism. The GAR-FTIR spectroscopy is based on measuring the reflectance−absorbance spectra of p-polarized light under the angle of incidence nearly parallel to a surface. It requires highly reflective mirror-like substrates, preferably consisting of an aluminum or gold layer.

FTIR characterization of organic monolayers on the diamond surface is not a trivial task. IR spectra are typically measured in a transmittance mode using KBr pellets containing diamond powders or free-standing substrate.[20,21] In both cases it is a time-consuming process which requires complex sample preparation prior to measurement. The KBr pellets must be carefully dried to avoid fingerprints of unwanted water-related bands in the final IR spectrum. IR spectra of the diamond can be also measured by ATR-FTIR using monocrystalline diamond in the form of prisms with one reflection. However, such materials are still expensive and too small, thus not allowing multiple reflections of ATR and often showing low sensitivity and low resolution.

Recently, we have introduced diamond-coated optical elements for ATR- and GAR-FTIR spectroscopy which offer simpler and faster sample preparation compared to transmission methods. In contrast to monocrystalline diamond, NCD layers are cheaper to be produced and can be deposited on various materials and over large areas. Such NCD layer also improves sample-to-sample reproducibility, and IR spectra can be recorded with high resolution. We have reported on the diamond-coated Si ATR prism, which was successfully used for the detection of the functional groups on the chemically modified diamond nanoparticles[22] and fetal bovine serum (FBS) proteins adsorbed on the oxidized diamond surface.[23] Moreover, we have shown that GAR-FTIR spectroscopy with diamond-coated Au optical mirrors could well resolve protein monolayers (about 3 nm thickness) adsorbed on the diamond surface.[24,25] The GAR-FTIR sensitivity was enhanced by choosing an optimized diamond surface morphology. However, the information about the influence of NCD surface functionalization on the protein adsorption is still missing.

In this manuscript we report on the GAR-FTIR characterization of the albumin binding to the amine-containing plasma polymer coatings deposited on the nanoporous diamond layers on Au mirrors. We show that enlarged surface area of the nanoporous diamond enhanced recognition of different functional groups on the very top surface of as-received, hydrogenated, and oxidized NCD layers. Moreover, diamond-coated GAR-IR element allowed us to study the intimate diamond-molecule interface. We present the IR spectra of PP on H- and O-terminated NCD layers and discuss its effect on the way of bovine serum albumin (BSA) adsorption, mainly on its morphology and increased adhesion. The GAR-FTIR data are corroborated by X-ray photoelectron spectroscopy (XPS) and atomic force microscopy (AFM). It is well-known that BSA represents the main inexpensive and water-soluble natural protein with good biocompatibility, which has been used for surface modification with various materials.[26,27] The covalent bonding typically requires the use of a suitable cross-linker molecule or adding specific functional groups on a molecule or surface. Amine is one common type of such functional cross-linking group. Therefore, in this work we have also involved the surface amination of the H- and O-terminated diamond surfaces by PP for further BSA adsorption studies. Understanding and controlling of the BSA adsorption and adhesion on the diamond surface is a key factor for many diverse applications building upon the unique diamond properties.

MATERIALS AND METHODS

Growth of NCD Layers. NCD layers (thickness about 100 nm) with flat or nanoporous surface morphologies were deposited on Si substrates and commercially available gold mirrors protected by silicon oxide (Thorlabs GmbH, Germany). Prior to the growth, the Si substrates and gold mirrors were seeded by diamond nanoparticles (nominal particle diameter 4.5 nm, NanoAmando, New Metals and Chemicals Corp. Ltd., Kyobashi) in an ultrasound bath. The diamond growth was realized in the large area linear antenna microwave plasma system (AK 400, Roth&Rau MicroSystems GmbH). NCD layers with flat morphology were grown from a hydrogen-rich gas mixture (10% CO_2 and 2.5% CH_4 in hydrogen) with a total process pressure 10 Pa, microwave power 1500 W, and temperature 280 °C. The nanoporous diamond layers were formed in two steps. First, thin continuous diamond films with the thickness of about 50 nm were formed by the hydrogen-based process gas mixture with 30% of CO_2 and 5% of CH_4. Afterward, the porous diamond layers were grown in oxygen-rich gas mixture with 80% of CO_2 and 20% of CH_4 with respect to H_2 flow with the following parameters: pressure 10 Pa, microwave power 2000 W, and temperature 350 °C. More detailed information on the growth of NCD layers can be found in ref 25.

SEM images and corresponding Raman spectra of flat and nanoporous NCD layers were previously presented.[25,13] The SEM images indicated porous or flat morphologies of NCD layers. Raman spectra revealed a diamond character of all layers (sharp peak centered at about 1330 cm^{-1} that corresponds to the sp^3 coordinated carbon) with some amount of sp^2 bonded carbon phase (the broad band near 1600 cm^{-1}).

Surface Functionalization of NCD Layers. Grown NCD layers were hydrogenated in pure hydrogen plasma (1500 W, 10 Pa, 200 °C, 1 h, AK 400 system, Roth&Rau MicroSystems, GmbH) to terminate the diamond surface with C−H surface groups and achieve hydrophobic surface properties. Part of such NCD samples was oxidized in a radio frequency oxygen plasma system (45 W, 50 Pa, 1 min, low pressure FEMTO system, Diener electronic GmbH & Co. KG) to modify the diamond surface with oxygen-containing surface groups and achieve hydrophilic surface properties. All H-NCD

DOI: 10.1021/acs.langmuir.9b02327
Langmuir XXXX, XXX, XXX−XXX

surfaces exhibited wetting angles approximately 100°, indicating highly hydrophobic surfaces. In contrast, the O-NCD surfaces showed a hydrophilic character with wetting angle below 5°.[25] A set of H-NCD and O-NCD samples was further functionalized with a thin (thickness about 7 ± 1 nm according to AFM measurements on planar monocrystalline diamond reference substrate) amine-containing PP prepared by RF magnetron sputtering of nylon 6,6 target in an Ar/N_2 (1:1) working gas mixture according to the protocol described in the literature.[13]

Proteins Adsorption on the Functionalized NCD Layers. Proteins were adsorbed on hydrogenated, oxidized, and aminated NCD surfaces from 15% Bovine Serum Albumin (BSA) solution in McCoy's 5A medium with stable glutamine without Phenol Red (BioConcept). BSA solution (100 μL) was dropped on the NCD surfaces, left for 10 min, rinsed with deionized water, and dried by nitrogen blow.

Characterization of Functionalized NCD Layers before and after BSA Adsorption. Infrared absorbance spectra of the functionalized NCD layers before and after the BSA adsorption were measured by GAR-FTIR spectroscopy. Measurements were performed using Thermo Nicolet 8700 spectrometer purged by nitrogen and equipped with MCT detector cooled by liquid nitrogen. Infrared spectra were recorded with p-polarized light at the Brewster's angle of diamond to suppress the interference fringes in the diamond layers. The optical absorbance of as-grown, hydrogenated, oxidized, and PP covered NCD layers was calculated as $A = -\log(R/R0)$, where R is the spectrum measured with NCD grown on protected gold mirror, $R0$ is the background spectrum recorded using a bare protected gold mirror. The optical absorbance of BSA, PP, and PP with adsorbed BSA proteins on the NCD surfaces was calculated as $A = -\log(R/R0)$, where R is the spectrum measured with BSA, PP, or PP with BSA, $R0$ is the background spectrum recorded using bare NCD layers grown on a protected gold mirror. In order to investigate the possible formation of new bonds at the interface between NCD and BSA, PP, and PP with adsorbed BSA, IR spectra were recorded using bare protected gold mirrors as backgrounds. All spectra represent an average of 128 scans recorded with a resolution of 4 cm^{-1}. More detailed information (schematic illustration and theoretical background) on the GAR-FTIR spectroscopy with diamond-coated Au mirrors was presented in our previous work.[25]

The surface chemical composition of the functionalized NCD layers before and after the BSA adsorption was characterized by X-ray photoelectron spectroscopy (XPS, Phoibos 150, Specs) using an Al Kα X-ray source (1486.6 eV, Specs). The XPS spectra were acquired at a constant takeoff angle of 90° with pass energy of 40 eV (wide spectra) and 10 eV (high resolution spectra). Peak fitting of the high resolution spectra was performed by the CasaXPS software using Shirley baseline and Gaussian line shapes of variable widths. The deviation of XPS peak fits was made with an accuracy of ±0.2 eV. The deconvolution description of the C 1s peaks of the samples and fitted C 1s peaks are shown in the Supporting Information.

Surface morphology and topography of BSA and PP on H- and O-terminated monocrystalline diamonds (MCD, purchased from Element Six) with atomically smooth surfaces were characterized using AFM. AFM measurements were performed in tapping, contact, and PFQNM[28] modes using Multi75Al cantilevers on ICON (Bruker) and Ntegra (NT-MDT) AFM systems. High resolution 1 × 1 μm^2 topography images were obtained in PFQNM mode on ICON (Bruker) AFM.

To determine a layer thickness, the contact mode (CM) nanoshaving procedure was performed on areas from 2 μm × 2 μm to 6 μm × 6 μm, i.e. several CM scans were made in different directions in order to move the PP or BSA layer to the edges, and overscan was made in tapping or PFQNM modes.[29] PP or BSA layer thickness was determined as the difference between the average surface height in the nanoshaved area and in the surrounding area. Root mean square (RMS) surface roughness was used as the error bar of surface height.

To determine the force required to remove the BSA, PP, or PP +BSA layers from the H-MCD and O-MCD surfaces, CM with increasing load (1−500 nN) was performed using Ntegra AFM on a 5 μm × 5 μm area with 0.5 Hz scan speed. The result was evaluated by AFM tapping mode across a 15 μm × 15 μm area. For force calibration, a nominal spring constant (k = 3 N/m) was used for all cantilevers. Due to the drift of reflected laser beam in relation to the photodiode, the error bar of the CM nanoshaving force is around 5 nN.

RESULTS AND DISCUSSION

Analysis of Hydrogenated and Oxidized NCD Layers. Infrared spectra of as-grown, H-NCD, and O-NCD layers with nanoporous morphologies are shown in Figure 1. The infrared

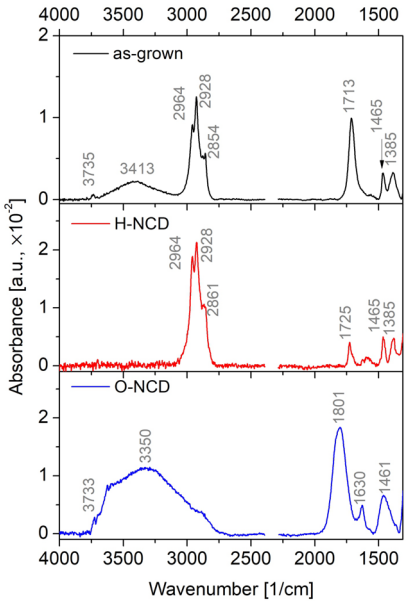

Figure 1. IR spectra of as-grown, H-NCD, and O-NCD layers with nanoporous morphologies (Au mirror used as the reference baseline).

spectrum of the as-grown NCD layer shows the presence of different hydrogen and oxygen containing functional groups. Three intense peaks in the region 2800−3000 cm^{-1} are related to the asymmetric and symmetric C−H stretching vibrations in CH_2 and CH_3 groups of sp^3 hybridized bonding.[30] Absorption bands at 3413 and 1713 cm^{-1} originate from the hydroxyl O−H and carbonyl C═O stretching vibrations, most probably involved in the carboxyl groups.[31] The weak bands appearing at 3735 and 1630 cm^{-1} are assigned to the O−H stretching and bending vibrations of physisorbed water on the diamond surface.[32] The peaks at 1465 and 1385 cm^{-1} correspond to the bending vibrations of CH_2 and CH_3 groups, respectively. The spectrum of H-NCD is dominated by the C−H groups. The O−H band at about 3400 cm^{-1} is almost vanishing, and only a residual carbonyl C═O peak at 1725 cm^{-1} is observed. In O-NCD layer, the contribution of the C−H groups is attenuated. The intensities of the O−H and C═O bands increased, indicating the chemisorption of the oxygen onto the diamond surface. The peak of the C═O stretching vibrations shifted from 1713 cm^{-1} for as-grown NCD to 1801 cm^{-1} for O-NCD layer. The data below 1200 cm^{-1} are not shown because of SiO_2 adsorption from protective layers on gold mirrors in this region.

The results of IR measurements on as-grown, H-NCD and O-NCD with flat surface morphologies are provided in the Supporting Information (Figure S1). These shows that GAR-

DOI: 10.1021/acs.langmuir.9b02327
Langmuir XXXX, XXX, XXX−XXX

Table 1. Concentration of the Chemical Elements and Chemical Bonds on the Surfaces of Flat and Nanoporous H-NCD and O-NCD Layers Calculated from XPS Spectra

		chemical elements, at. %			chemical bonds, %			
sample name	type of morphology	O	C	Si	sp^2 (C═C)	sp^3 (C−C, C−H)	C−O	C═O
H-NCD	flat	5	95		2	88	10	
O-NCD		11	89		13	68	16	3
H-NCD	nanoporous	11	84	5	2	91	7	
O-NCD		22	75	4	18	64	14	4

FTIR on flat NCD layers deposited on protected Au mirrors was not sensitive enough to detect the functional groups covalently bonded to the diamond surface. Measured spectra did not show any peaks.

Thus, GAR-FTIR with nanoporous NCD layers was the only sensitive method to characterize the very top surface of the diamond after plasma modification. IR spectra with high resolution clearly show the difference in the functional groups on as-grown, hydrogenated, and oxidized NCD surfaces (Figure 1). The surface of H-NCD layers is dominated by hydrogen bonds with a residual amount of carbonyl groups. After the plasma oxidation, the surface of O-NCD layers is dominated by oxygen-containing functional groups. The IR spectra of nanoporous NCD layers also corroborate by the XPS analyses (Figure S2c, d).

The concentration of the chemical elements and chemical bonds on the surfaces of flat (Figure S2a, b) and nanoporous (Figure S2c, d) H-NCD and O-NCD layers as calculated from XPS spectra is summarized in Table 1. It shows that the flat H-NCD layers contain 5 at. % of oxygen and 95 at. % of carbon. The flat O-NCD layers contain 11 at. % of oxygen and 89 at. % of carbon. The concentration of C−O bonds is 10% and 16% on the surfaces of H-NCD and O-NCD, respectively. On the surfaces of nanoporous NCD layers the concentration of oxygen was 11 and 22 at. % for H-NCD and O-NCD layers, respectively. On both nanoporous H-NCD and O-NCD layers, the presence of Si coming from the protective SiO_2 layer was also detected. The concentration of the C−O bonds on the nanoporous H-NCD and O-NCD layers was 7% and 14%, respectively. Note, however, that in the case of nanoporous NCD layers the quality of XPS spectra was influenced by the rough structure of the samples and also by the signal from the Si based protective layer deposited on the Au mirror which prohibits the qualified interpretation of the obtained XPS data.

BSA Adsorption on the Hydrogenated and Oxidized Diamond Surfaces. H-NCD and O-NCD layers with well-defined surface properties were further used for the adsorption of BSA proteins. Figure 2 shows IR spectra of BSA proteins adsorbed on the nanoporous H-NCD and O-NCD surfaces and IR spectra of H-NCD+BSA and O-NCD+BSA interfaces. Infrared spectra of bare H-NCD and O-NCD layers are also added for comparison.

IR spectra of both H-NCD+BSA and O-NCD+BSA interfaces (Figure 2) show a combination of the functional groups in the diamond and BSA proteins. In the case of H-NCD, C−H vibrations represent a mixed signal from the diamond surface and BSA proteins. In the spectrum of O-NCD layers the C═O related peak at 1786 cm^{-1} is preserved after BSA adsorption and C−H groups appear due to BSA adsorption. Deconvolution of both spectra did not indicate the formation of new bonds between the diamond and BSA proteins. However, there is an obvious qualitative difference in the region 1300−1700 cm^{-1} that again indicates a different

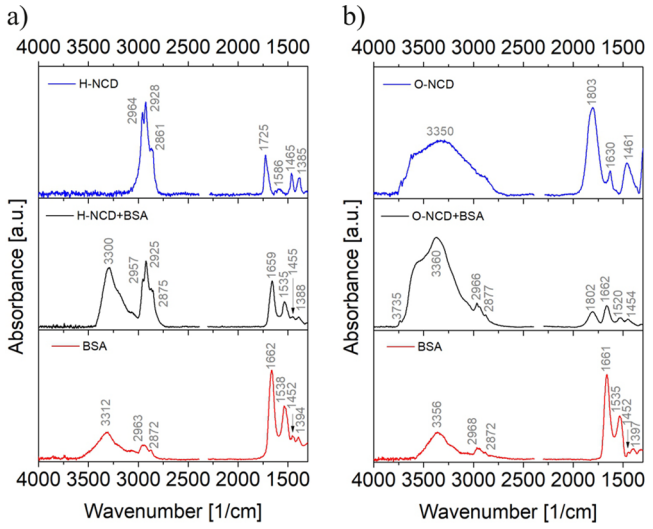

Figure 2. IR spectra of (a) H-NCD and (b) O-NCD nanoporous layers before and after BSA adsorption (Au mirror used as the reference baselines). IR spectra of BSA adsorbed on H-NCD or O-NCD nanoporous layers (NCD used as the reference baselines).

BSA arrangement on H-NCD and O-NCD, in similarity to other molecules.[33]

Infrared spectra of BSA adsorbed on both H-NCD and O-NCD show the presence of the band near 3300 cm^{-1} related to N−H stretching vibrations and O−H stretching vibrations of adsorbed water. The band of very weak adsorption at 3050 cm^{-1} is related to overtone of the amide II band. Peaks near 3000 cm^{-1} are related to C−H stretching vibrations. The peak near 1660 cm^{-1} is the amide I band, which results from the C═O stretching vibrations. The peak near 1540 cm^{-1} is called the amide II band and is related to N−H bending and C−N stretching vibrations.[34,35] The peak at 1450 cm^{-1} results from the protein side-chain. The amide III band near 1300 cm^{-1} is related to C−N stretching and N−H bending vibrations. These bands near 1400 cm^{-1} may be also related to C−H bending vibrations. The C−H vibrations near 1400 and 3000 cm^{-1} are less pronounced for BSA on O-NCD. This effect could be explained by the formation of the hydrogen bond between oxygen surface groups on diamond with C−H groups on BSA.

The concentration of the chemical elements and bonds on the flat H-NCD and O-NCD layers after BSA adsorption calculated from XPS spectra is summarized in Table 2. The deconvolutions of the C 1s peaks are shown in Figure S3a, b. The concentration of nitrogen on H-NCD and O-NCD surfaces after BSA adsorption was about 6 and 7 at. %, respectively. Components C−N, C═N, and CN in deconvolution are generalized by the abbreviation "CN". The total concentrations of C−O and CN bonds on the surface of BSA adsorbed on the H-NCD and O-NCD are 8% and 4%,

DOI: 10.1021/acs.langmuir.9b02327
Langmuir XXXX, XXX, XXX−XXX

Table 2. Concentration of the Chemical Elements and Bonds on the Flat H-NCD and O-NCD Layers after BSA Adsorption Calculated from XPS Spectra

	chemical elements, at %				chemical bonds, %				
sample name	O	C	N	Au	sp^2 (C≡C)	sp^3 (C−C, C−H)	C−O, CN	C═O, N−C═O	O−C═O
H-NCD/BSA	10	84	6		6	47	8	19	20
O-NCD/BSA	15	78	7		14	44	4	15	23

respectively. Please note that XPS cannot distinguish the carbon from biomolecules and diamond background. This indicates that BSA is present on both diamond types in a similar amount.

High resolution AFM topography images of BSA proteins on H- and O-terminated atomically smooth monocrystalline diamond (MCD) surfaces (Figure 3a, b) show that BSA adsorbed on H-MCD looks like a layer with holes, while on O-MCD it looks like the presence of small spherical nanoparticles. RMS roughness of the BSA layer is 0.7 and 0.9 nm on H-MCD and O-MCD surfaces, respectively.

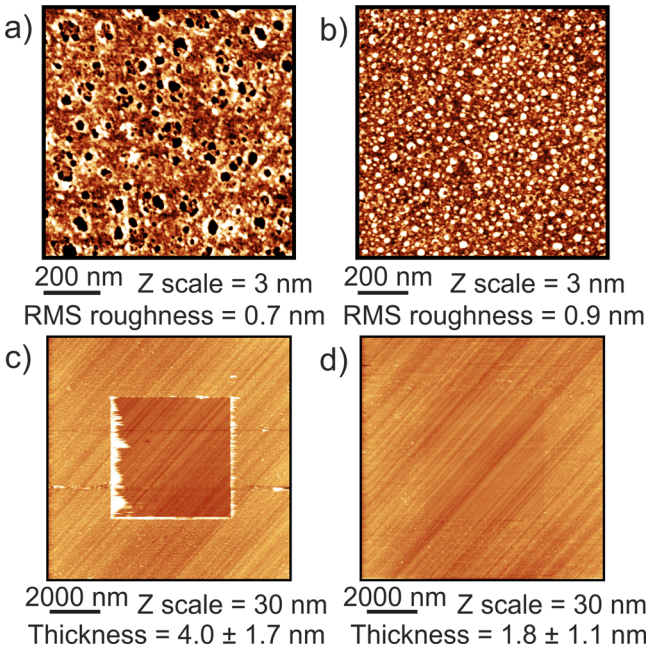

Figure 3. High resolution AFM topography images and result of CM nanoshaving of BSA proteins adsorbed on H-MCD (a, c) and O-MCD (b, d) surfaces.

Results of CM nanoshaving (Figure 3c, d) show that the thickness of BSA layer is 4.0 ± 1.7 nm on the H-MCD surface and 1.8 ± 1.1 nm on the O-MCD surface. CM with increasing load (see Supporting Information, Figure S4) shows that the force required to remove the BSA from H-MCD surface was 10 ± 5 nN. The force required to remove the BSA from O-MCD surface was 20 ± 5 nN. Relatively small nanoshaving forces also suggest that BSA is merely physisorbed on both H-MCD and O-MCD surfaces and no covalent attachment is formed. Still the difference in nanoshaving forces confirms different arrangement and different interaction of BSA with H-NCD and O-NCD substrates as suggested by AFM morphology and IR spectra.

BSA Adsorption on the Diamond Aminated from the Plasma Polymer. Figure 4 shows the IR spectra of PP on nanoporous H-NCD and O-NCD layers before and after adsorption of BSA proteins. The IR spectra of PP on both H-NCD and O-NCD layers indicate the presence of adsorption band at ~3300 cm^{-1}, which we assign to N−H stretching overlapped with O−H stretching. Peaks near 3000, 1450, and 1390 cm^{-1} are related to C−H stretching and bending vibrations. The band at 2174 cm^{-1} corresponds to the vibration of C≡N and C≡C groups. The peak near 1670 cm^{-1} is related to the stretching vibrations of C−N, C═O, and C═C bonds. Yet the PP spectra are still noticeably different. The PP on the H-NCD layer seems to contain more C≡N, C≡C, and C−H groups compared to PP on the O-NCD layer. Such often positively charged functional groups tend to create hydrogen bonds or more generally electrostatic bonds with negatively charged O-NCD surface groups. Therefore, their vibrations are diminished on O-NCD. Such interactions could lead to slightly different growth of PP on O-NCD compared to H-NCD. A similar effect of diamond surface termination on the growth of macromolecules was

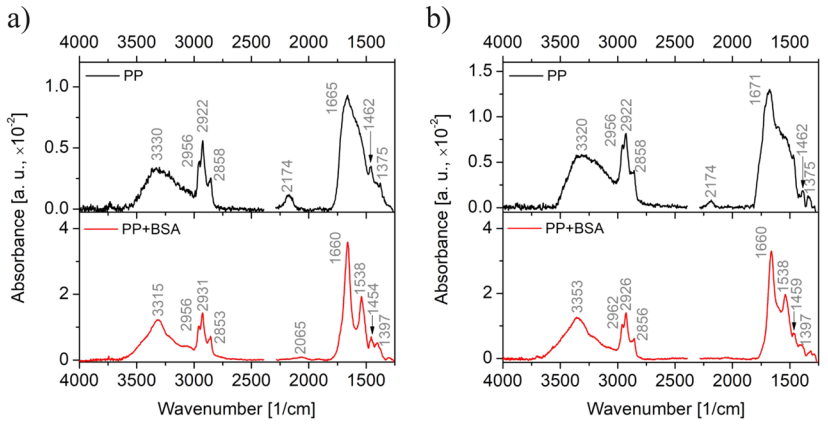

Figure 4. IR spectra of PP before and after BSA adsorption on (a) H-NCD and (b) O-NCD nanoporous layers. NCD used as the reference baseline.

DOI: 10.1021/acs.langmuir.9b02327
Langmuir XXXX, XXX, XXX−XXX

Table 3. Concentration of the Chemical Elements and Bonds on the Flat H-NCD and O-NCD Surfaces after Amination with PP and BSA Adsorption Calculated from XPS Spectra

	chemical elements, at. %			chemical bonds, %			
sample name	O	C	N	C−C, C−H	C−O, CN	C═O, N—C═O	O—C═O
H-NCD/PP	16	55	29	32	37	29	3
O-NCD/PP	16	55	29	53	34	12	1
Au/PP	11	55	34	27	43	30	
H-NCD/PP/BSA	19	60	21	42	31	26	1
O-NCD/PP/BSA	19	59	22	52	30	17	1
Au/PP/BSA	13	62	25	40	29	31	

reported for pentacene.[36] A representative SEM image (taken at an angle of 45°) of the nanoporous H-NCD layer covered with PP and the adsorbed BSA protein layer is shown in the Supporting Information (Figure S5).

Infrared spectra of PP with adsorbed BSA proteins are dominated by the amine-containing functional groups typical for BSA proteins. The spectra seem to be very similar on both H-NCD and O-NCD. A slight difference in the peak intensities near 1400 cm^{-1} (COO−, C−N, N−H, and C−H) is obviously related with the difference in PP spectra in that region, not with difference in BSA bonding to PP.

IR spectra of H-NCD+PP and O-NCD+PP interfaces before and after BSA adsorption where Au was used as the baseline are shown in the Supporting Information (Figure S6).

The concentration of the chemical elements and bonds on the flat NCD layers after amination with PP and BSA adsorption calculated from XPS spectra is summarized in Table 3. The deconvolutions of the C 1s peaks represented in Figure S7a−f. The data for reference measurements of Au mirrors with and without the PP and BSA proteins are added for a comparison (Figure S8a−c). In the case of the reference Au/BSA sample, a strong signal from an Au substrate (about 22 at. %) was detected by XPS due to the rather thin (about 2 nm thick) layer of BSA adsorbed on Au substrate (Figure S8b).

It is clearly visible that both H-NCD and O-NCD layers covered with PP showed 29 at. % of nitrogen. This value is comparable with nitrogen concentration (34 at. %) measured on the surface of the PP deposited on Au substrates. Components C−N, C═N, and C≡N in deconvolution are generalized by the abbreviation "CN". Deconvolution of the C 1s XPS high resolution spectra showed the presence of nitrogen-containing bonds on the surface of H-NCD and O-NCD layers after amination. The total concentration of C−O and CN bonds changed to 37% and 34% for H-NCD and O-NCD layers, indicating the presence of CN bonds on both diamond types. To conclude, both NCD with PP reveals the same O at. % and the same N at. %. In addition, the thickness of PP is about 7 nm, as found by AFM. The XPS penetration depth is about a few nm from the top of the sample surface. As a consequence, it is not possible to reach the interface between the PP and NCD layer. This all means that (a) XPS detects signal only from PP (not from diamond) and (b) the PP contains also amine groups.

NCD layers with PP and adsorbed BSA proteins contained about 22 at. % of nitrogen, which is lower than on PP without BSA. The concentration of oxygen increased in both H- and O-NCD surfaces after BSA adsorption. After BSA adsorption on PP, the total concentration of C−O and CN bonds was 31% and 30% for H-NCD and O-NCD layers, respectively. These values are comparable with the total concentration of C−O and CN bonds (29%) on the surface of the PP and BSA proteins deposited on Au substrates. In addition, AFM shows BSA thickness is 2−4 nm. Thus BSA becomes significant part within XPS penetration depth (5−7 nm). This all means that the XPS measurements indicate presence of BSA on the PP because BSA contains less nitrogen (amine groups) and more oxygen containing groups. This conclusion is confirmed by the same trends of oxygen increase and nitrogen decrease on the Au reference samples.

High resolution AFM topography images and the results of CM nanoshaving of PP before and after BSA adsorption on H-MCD and O-MCD surfaces are presented in Figure 5. High resolution AFM topography images show that PP forms a flat layer on the O-MCD surface, while it is rougher on the H-MCD surface. The RMS roughness of PP is 0.4 nm on O-MCD and 0.7 nm on H-MCD surfaces. The layers of PP with adsorbed BSA show the presence of small particles on both O-MCD and H-MCD surfaces. RMS roughness of PP with adsorbed BSA is 0.6 nm on both H-MCD and O-MCD surfaces.

The results of CM nanoshaving show that the thickness of the PP layer is around 6−7 nm on both O-MCD and H-MCD surfaces. The thickness of PP with adsorbed BSA is 10.3 ± 0.7 nm on H-MCD and 8.8 ± 1.5 nm on O-MCD surfaces. AFM is well correlated with IR and XPS data indicating different surface morphologies of the PP and BSA proteins on H-MCD and O-MCD surfaces. It is most probably influenced by the diamond hydrophobic (H-NCD layers with wetting angle about 100°) or hydrophilic (O-NCD layers with wetting angle about 10°) surface properties. Such high hydrophobicity is correlated with missing OH band in IR spectra of nanoporous H-NCD layers. This is most likely due to the nanoporous structure of diamond.

The morphology of the PP with adsorbed BSA is the same on both H-MCD and O-MCD surfaces. This happened because the surface properties of the top part of the PP layer are the same and do not depend on the surface termination of the diamond. Hence, BSA molecules have the same surface below them and thus they form layers with similar morphology. CM nanoshaving with increasing load (see Supporting Information, Figure S4) indicated that the force required to remove the PP from both H-MCD and O-MCD was 300 nN. The force required to remove the PP with adsorbed BSA from both H-MCD and O-MCD was 250 nN. Several additional measurements confirmed that with lower applied force 150−200 nN the BSA layer slightly moved on the PP but was not completely removed. With force below 200 nN the BSA layer was slightly damaged but not removed from the PP. Measurements on H-MCD and O-MCD surfaces with PP and PP with adsorbed BSA were performed using the same tip.

The force 300 nN required to remove the PP from H-MCD and O-MCD surfaces is higher than the force which was

DOI: 10.1021/acs.langmuir.9b02327
Langmuir XXXX, XXX, XXX−XXX

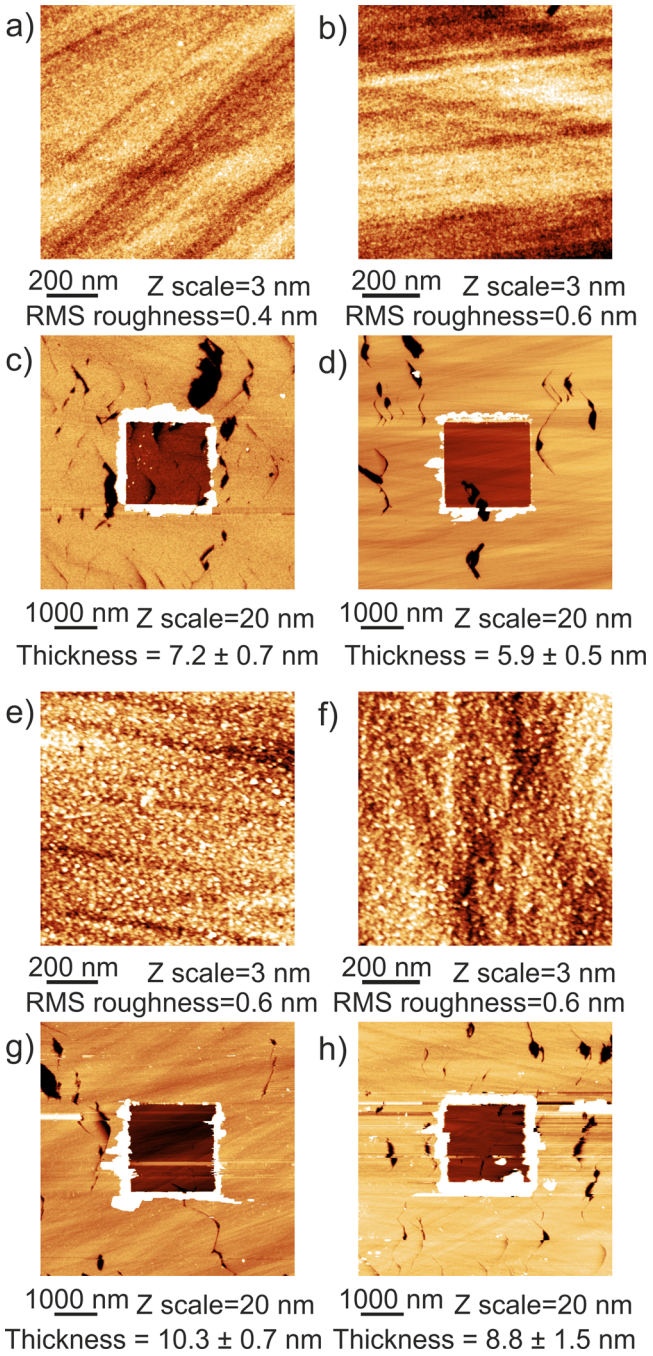

Figure 5. High resolution AFM topography images and the result of CM nanoshaving of PP before (a–d) and after (e–h) BSA adsorption on H-MCD (a, c, e, g) and O-MCD (b, d, f, g) surfaces.

required to remove covalently attached DNA from the diamond (45–76 nN).[28] One possibility is that PP could be covalently attached to both hydrogen and oxygen terminated diamonds. Such grafting is, however, unlikely to occur on such different surface groups. A more likely explanation is that such high force is caused by PP cross-linking, i.e. the AFM tip needs first to penetrate the rigid PP layer to remove it from the diamond surface.

Moreover, AFM data show that the BSA layer cannot be removed from the PP layer, the layer is removed as a whole. This can happen either because of the covalent bonding between BSA and PP or because of the tight BSA encapsulation in PP. Experiments with BSA adsorption on aminated monocrystalline diamond (i.e., diamond processed by RF plasma treatment in ammonia, see Figure S9 in the Supporting Information) show only small CM nanoshaving forces (10–15 nN). Covalent bonding of BSA to amine-containing PP is thus also unlikely. This is supported also by the IR spectra as discussed above. PP thus provides a strong interlink between BSA and diamond while preserving BSA morphology and therefore functionality (unlike when BSA is adsorbed directly on H-NCD).

CONCLUSIONS

Flat and nanoporous diamond layers grown on Au mirrors were successfully used as the functional layer for the investigation of bovine serum albumin (BSA) protein (2–4 nm) using complementary analytic techniques (FTIR, XPS, and AFM). The nanoporous diamond morphology resulted in a better recognition of amine-containing groups by GAR-FTIR measurements. Next, the BSA adhesion was also significantly influenced by the diamond surface termination (hydrogen, oxygen, and amine-containing plasma polymer (PP) interlayer).

Infrared spectra correlated well with XPS data confirming higher concentrations of the C–H and nitrogen-containing bonds on H-NCD layers after BSA protein adsorption. Obtained differences in nanoshaving forces for BSA proteins on the H- and O-terminated NCD layers indirectly indicated different arrangements of molecules at the top of the diamond surface. Moreover, these measurements revealed most probably only the result of physisorption instead of any covalent attachment.

In the case of employing the PP interlayer on the H- and O-terminated diamond surfaces, GAR-FTIR and XPS measurements revealed similar trends in chemical compositions after the BSA protein adhesion. Similarly, morphologies and nanoshaving force measurements of the PP with adsorbed BSA were nearly identical for both NCD terminations. Thus, the PP interlayer was thick enough to suppress any influence of H- or O-terminated NCD on BSA adsorption. The PP interlayer provided only a strong interlink between BSA and diamond while preserving its globular conformation and probably also its biochemical functionality, which is in contrast to when BSA is adsorbed directly on the H-NCD.

Based on the presented results, the thin (7 nm) PP layer can be used as the interlayer which greatly improves the adhesion strength between the BSA and diamond. This concept can be used in many applications, which deal, for example, with cell adhesion and require the presence of BSA during cell growth. As has been demonstrated earlier,[13] the surface conductivity of the H-terminated NCD layer is preserved after the deposition of the PP interlayer. Moreover, PP showed good surface chemical stability after different sterilization methods.[12] Thus, all these factors make the nanoporous H-NCD aminated with PP a very promising functional layer for biosensor applications.

ASSOCIATED CONTENT

Supporting Information

The Supporting Information is available free of charge on the ACS Publications website at DOI: 10.1021/acs.langmuir.9b02327.

DOI: 10.1021/acs.langmuir.9b02327
Langmuir XXXX, XXX, XXX–XXX

GAR-FTIR spectra, XPS data, AFM images, and more details about BSA adsorption on the diamond aminated from the PP (PDF)

AUTHOR INFORMATION

Corresponding Author

*Email: kozak@fzu.cz.

ORCID

Halyna Kozak: 0000-0003-3935-0094

Notes

The authors declare no competing financial interest.

ACKNOWLEDGMENTS

We acknowledge Rajisa Jackivova for oxygen plasma treatment and SEM measurements and Marie Kalbáčová for BSA donation. This work was supported by Operational Programme Research, Development and Education financed by European Structural and Investment Funds and the Czech Ministry of Education, Youth and Sports (Project No. SOLID21-CZ.02.1.01/0.0/0.0/16_019/0000760), by LNSM project, and by project GACR 17-19968S (B.R.).

REFERENCES

(1) Buchmann, P. K. Properties and Applications of Diamond, by J. Wilks Und E. Wilks, Butterworth-Heinemann, Oxford 1991 525 Pp., Hardcover, ISBN 0−7506−1067−0. *Adv. Mater.* **1992**, *4* (4), 307−307.

(2) Pan, L. S., Kania, D. R. *Diamond: Electronic Properties and Applications*; Electronic Materials: Science & Technology; Springer US, 1995.

(3) Yang, W.; Auciello, O.; Butler, J. E.; Cai, W.; Carlisle, J. A.; Gerbi, J. E.; Gruen, D. M.; Knickerbocker, T.; Lasseter, T. L.; Russell, J. N.; et al. DNA-Modified Nanocrystalline Diamond Thin-Films as Stable. *Nat. Mater.* **2002**, *1* (4), 253−257.

(4) Szunerits, S.; Boukherroub, R. Different Strategies for Functionalization of Diamond Surfaces. *J. Solid State Electrochem.* **2008**, *12* (10), 1205−1218.

(5) Maier, F.; Riedel, M.; Mantel, B.; Ristein, J.; Ley, L. Origin of Surface Conductivity in Diamond. *Phys. Rev. Lett.* **2000**, *85* (16), 3472−3475.

(6) Landstrass, M. I.; Ravi, K. V. Hydrogen Passivation of Electrically Active Defects in Diamond. *Appl. Phys. Lett.* **1989**, *55* (14), 1391−1393.

(7) Rezek, B.; Michalíková, L.; Ukraintsev, E.; Kromka, A.; Kalbacova, M. Micro-Pattern Guided Adhesion of Osteoblasts on Diamond Surfaces. *Sensors* **2009**, *9* (5), 3549−3562.

(8) Koch, H.; Kulisch, W.; Popov, C.; Merz, R.; Merz, B.; Reithmaier, J. P. Plasma Amination of Ultrananocrystalline Diamond/Amorphous Carbon Composite Films for the Attachment of Biomolecules. *Diamond Relat. Mater.* **2011**, *20* (2), 254−258.

(9) Stateva, S.; Merker, D.; Popov, C.; Apostolova, M. Ultrananocrystalline Diamond Coated Implants for Enhanced Osseointegration. *BioDiscovery* **2017**, *20*, No. e19830.

(10) Wei, J. J.; Liu, J. L.; Chen, L. X.; Hei, L. F.; Lv, F. X.; Li, C. M. Amination of Diamond Film by Ammonia Microwave Plasma Treatment. *Diamond Relat. Mater.* **2015**, *54*, 34−38.

(11) Kozak, H.; Remes, Z.; Kromka, A.; Ledinsky, M. Optical Characterisation of Organosilane-Modified Nanocrystalline Diamond Films. *Chem. Pap.* **2011**, *65* (1), 34−38.

(12) Artemenko, A.; Kylián, O.; Choukourov, A.; Gordeev, I.; Petr, M.; Vandrovcová, M.; Polonskyi, O.; Bačáková, L.; Slavinska, D.; Biederman, H. Effect of Sterilization Procedures on Properties of Plasma Polymers Relevant to Biomedical Applications. *Thin Solid Films* **2012**, *520* (24), 7115−7124.

(13) Artemenko, A.; Kozak, H.; Biederman, H.; Choukourov, A.; Kromka, A. Amination of NCD Films for Possible Application in Biosensing. *Plasma Processes Polym.* **2015**, *12* (4), 336−346.

(14) Kozak, H.; Kromka, A.; Ledinsky, M.; Rezek, B. Enhancing Nanocrystalline Diamond Surface Conductivity by Deposition Temperature and Chemical Post-Processing. *Phys. Status Solidi A* **2009**, *206* (2), 276−280.

(15) Kozak, H.; Kromka, A.; Babchenko, O.; Rezek, B. Directly Grown Nanocrystalline Diamond Field-Effect Transistor Microstructures. *Sens. Lett.* **2010**, *8* (3), 482−487.

(16) Agashe, M.; Raut, V.; Stuart, S. J.; Latour, R. A. Molecular Simulation to Characterize the Adsorption Behavior of a Fibrinogen Gamma-Chain Fragment. *Langmuir* **2005**, *21* (3), 1103−1117.

(17) Wilson, C. J.; Clegg, R. E.; Leavesley, D. I.; Pearcy, M. J. Mediation of Biomaterial-Cell Interactions by Adsorbed Proteins: A Review. *Tissue Eng.* **2005**, *11* (1−2), 1−18.

(18) Sabbatini, S.; Conti, C.; Orilisi, G.; Giorgini, E. Infrared Spectroscopy as a New Tool for Studying Single Living Cells: Is There a Niche? *Biomed. Spectrosc. Imaging* **2017**, *6* (3−4), 85−99.

(19) Barth, A. Infrared Spectroscopy of Proteins. *Biochim. Biophys. Acta, Bioenerg.* **2007**, *1767* (9), 1073−1101.

(20) Girard, H. A.; Arnault, J. C.; Perruchas, S.; Saada, S.; Gacoin, T.; Boilot, J.-P.; Bergonzo, P. Hydrogenation of Nanodiamonds Using MPCVD: A New Route toward Organic Functionalization. *Diamond Relat. Mater.* **2010**, *19* (7−9), 1117−1123.

(21) Titus, E.; Singh, M.; Unni, K. N.; Tyagi, P.; Dua, A.; Roy, M.; Misra, D. Diamond Nucleation and Growth on Zeolites. *Diamond Relat. Mater.* **2003**, *12* (10−11), 1647−1652.

(22) Remes, Z.; Kozak, H.; Rezek, B.; Ukraintsev, E.; Babchenko, O.; Kromka, A.; Girard, H. A.; Arnault, J.-C.; Bergonzo, P. Diamond-Coated ATR Prism for Infrared Absorption Spectroscopy of Surface-Modified Diamond Nanoparticles. *Appl. Surf. Sci.* **2013**, *270*, 411−417.

(23) Izak, T.; Babchenko, O.; Potocky, S.; Remes, Z.; Kozak, H.; Verveniotis, E.; Rezek, B.; Kromka, A. CHAPTER 13:Low Temperature Diamond Growth. *In Nanodiamond* **2014**, 290−342.

(24) Remes, Z.; Kozak, H.; Babchenko, O.; Potocky, S.; Ukraintsev, E.; Rezek, B.; Kromka, A. Grazing Angle Reflectance Spectroscopy of Organic Monolayers on Nanocrystalline Diamond Films. *Diamond Relat. Mater.* **2011**, *20* (7), 882−885.

(25) Kozak, H.; Babchenko, O.; Artemenko, A.; Ukraintsev, E.; Remes, Z.; Rezek, B.; Kromka, A. Nanostructured Diamond Layers Enhance the Infrared Spectroscopy of Biomolecules. *Langmuir* **2014**, *30* (8), 2054−2060.

(26) Purohit, R.; Vallabani, N.; Shukla, R. K.; Kumar, A.; Dhawan, A.; Singh, S. BSA Coated Gold Nanoparticles Exhibit Size Dependent Interaction with Lung Cancer (A549) Cells. *Mol. Cytogenet.* **2014**, *7*, P83.

(27) Du, J.; Li, B.; Zhang, P.; Wang, Y. Cationized Bovine Serum Albumin as Gene Carrier: Influence of Specific Secondary Structure on DNA Complexibility and Gene Transfection. *Colloids Surf., B* **2016**, *143*, 37−46.

(28) Rezek, B.; Ukraintsev, E.; Krátká, M.; Taylor, A.; Fendrych, F.; Mandys, V. Epithelial Cell Morphology and Adhesion on Diamond Films Deposited and Chemically Modified by Plasma Processes. *Biointerphases* **2014**, *9* (3), No. 031012.

(29) Rezek, B.; Ukraintsev, E.; Kromka, A.; Ledinský, M.; Brož, A.; Nosková, L.; Hartmannová, H.; Kalbacova, M. Assembly of Osteoblastic Cell Micro-Arrays on Diamond Guided by Protein Pre-Adsorption. *Diamond Relat. Mater.* **2010**, *19* (2−3), 153−157.

(30) Ando, T.; Yamamoto, K.; Ishii, M.; Kamo, M.; Sato, Y. Vapour-Phase Oxidation of Diamond Surfaces in O2 Studied by Diffuse Reflectance Fourier-Transform Infrared and Temperture-Programmed Desorption Spectroscopy. *J. Chem. Soc., Faraday Trans.* **1993**, *89* (19), 3635−3640.

(31) Socrates, G.; Socrates, G. *Infrared and Raman Characteristic Group Frequencies: Tables and Charts*, 3rd ed.; Wiley: Chichester; New York, 2001.

DOI: 10.1021/acs.langmuir.9b02327
Langmuir XXXX, XXX, XXX−XXX

(32) Mochalin, V.; Osswald, S.; Gogotsi, Y. Contribution of Functional Groups to the Raman Spectrum of Nanodiamond Powders. *Chem. Mater.* **2009**, *21* (2), 273−279.
(33) Miliaieva, D.; Stehlik, S.; Stenclova, P.; Rezek, B. Synthesis of Polypyrrole on Nanodiamonds with Hydrogenated and Oxidized Surfaces: Synthesis of Polypyrrole on Nanodiamonds. *Phys. Status Solidi A* **2016**, *213* (10), 2687−2692.
(34) Maruyama, T. FT-IR Analysis of BSA Fouled on Ultrafiltration and Microfiltration Membranes. *J. Membr. Sci.* **2001**, *192* (1−2), 201−207.
(35) Li, Z.; Qiang, L.; Zhong, S.; Wang, H.; Cui, X. Synthesis and Characterization of Monodisperse Magnetic Fe3O4@BSA Core−Shell Nanoparticles. *Colloids Surf., A* **2013**, *436*, 1145−1151.
(36) Gajewski, W.; Huth, M.; Buth, F.; Nickel, B.; Stutzmann, M.; Garrido, J. A. Photoresponse and Morphology of Pentacene Thin Films Modified by Oxidized and Reduced Diamond Surfaces. *Phys. Rev. B: Condens. Matter Mater. Phys.* **2009**, *80* (23), 235311-6.

DOI: 10.1021/acs.langmuir.9b02327
Langmuir XXXX, XXX, XXX−XXX